ML-assisted Equalization for 50-Gb/s/λ O-band CWDM Transmission over 100-km SMF

Yang Hong, *Member, IEEE*, Stavros Deligiannidis, Natsupa Taengnoi, Kyle R. H. Bottrill, Naresh K. Thipparapu, Yu Wang, Jayanta K. Sahu, David J. Richardson, *Fellow, IEEE*, Charis Mesaritakis, Adonis Bogris, *Senior Member, OSA*, and Periklis Petropoulos, *Fellow, OSA*

***Abstract*—We propose and demonstrate a bidirectional Vanilla recurrent neural network (Vanilla-RNN) based equalization scheme for O-band coarse wavelength division multiplexed (CWDM) transmission. Based on a 4×50-Gb/s intensity modulation and direct detection (IM/DD) system, we demonstrate the significantly better bit error rate (BER) performance of the Vanilla-RNN scheme over the conventional decision feedback equalizer (DFE) for both Nyquist on-off keying (OOK) and Nyquist 4-ary pulse amplitude modulation (PAM4) formats. It is shown that the Vanilla-RNN equalizer is capable of compensating for both linear and nonlinear impairments induced by the transceiver and the single-mode fiber (SMF). As a result, up to 100-km and 75-km SMF transmission can be achieved for OOK and PAM4 transmission, respectively. Furthermore, through the comparison with other equalization schemes, including the linear equalizer, 3rd-order Volterra equalizer, and Volterra+DFE, it is demonstrated that the Vanilla-RNN equalizer achieves the best BER performance. In the meantime, it also exhibits lower implementation complexity when compared to Volterra-based schemes. Our results show that the Vanilla-RNN scheme is a viable solution for realizing simple and effective equalization. This work serves as an exploration and offers useful insights for future implementations of reach-extended O-band CWDM IM/DD systems.**

***Index Terms*—Machine Learning; O-band Transmission; Intensity-modulation and Direct-detection; Coarse Wavelength-division Multiplexing.**

Manuscript was received XX xx, 2021. This work was supported by the UK's EPSRC under the *Airguide Photonics* Programme Grant (EP/P030181/1), and projects *COALESCE* (EP/P003990/1) and PHOS (EP/S002871/1), and by the Hellenic Foundation for Research and Innovation (H.F.R.I.) under the "2nd Call for H.F.R.I. Research Projects to support Faculty Members & Researchers" (Project Number: 2901). (Corresponding authors: *Y. Hong* and *S. Deligiannidis*).

Y. Hong, N. Taengnoi, K. R. H. Bottrill, N. K. Thipparapu, Y. Wang, J. K. Sahu, D. J. Richardson, and P. Petropoulos are with the Optoelectronics Research Centre (ORC), University of Southampton, Southampton SO17 1BJ, United Kingdom. (e-mails: y.hong@soton.ac.uk; nt1a15@soton.ac.uk; k.bottrill@soton.ac.uk; nkt1d17@soton.ac.uk; yw9n17@soton.ac.uk; jks@orc.soton.ac.uk; djr@orc.soton.ac.uk; pp@orc.soton.ac.uk)

S. Deligiannidis, and A. Bogris are with the Department of Informatics and Computer Engineering, University of West Attica, Aghiou Spiridonos, Egaleo, 12243, Greece. (e-mails: sdeligiannid@uniwa.gr; abogris@uniwa.gr)

C. Mesaritakis is with the Department of Information and Communication Systems Engineering, University of the Aegean, Palama 2, Samos-83200, Greece. (e-mail: cmesar@aegean.gr)

I. Introduction

MACHINE learning (ML) has been attracting extensive interest from both academia and industry in the optical communications community in recent years [1]. A wide range of applications that exploit the use of ML have been reported, including optical performance monitoring, optimization of optical networks, fault management in optical networks, optimization of the design of physical-layer systems and components, and advanced digital signal processing [2-4].

Amongst these applications, ML-assisted equalization has been considered as a promising solution to realize the recovery of targeted signals. While it is challenging for traditional equalization schemes to simultaneously accommodate the channel impairments induced by chromatic dispersion (CD) in single-mode fibers (SMFs), the interplay between square-law detection and the chirping in the lasers/modulators, as well as the addition of noise in the system [5-7], ML techniques have demonstrated excellent capability to mitigate both linear and nonlinear distortions in optical transmission systems [8-11]. In [8], an end-to-end deep neural network (NN) based scheme was demonstrated in a single-wavelength C-band intensity modulation and direct detection (IM/DD) system, showing superior bit error rate (BER) performance compared to linear feedforward equalization (FFE). A NN-based equalization scheme was evaluated in a C-band passive optical network system in [9], wherein it was shown that the NN-based equalizer, while having similar equalization performance to the linear FFE and Volterra nonlinear equalization with regard to linear distortions, exhibited much better performance under nonlinear distortions.

While most of the previous works focused on the use of ML-based equalization in the C-band, the use of ML-based equalization is even more desirable in the O-band, especially in emerging amplified wavelength-division multiplexed (WDM) systems, where the nonlinearity issue in these systems may become more pronounced due to the low CD in this spectral region [12, 13]. While the O-band is generally specified for use in short-reach applications, the recent emergence of bismuth-doped fiber amplifiers (BDFAs) has enabled a substantial extension of the achievable reach [14-16]. However, only a few works on ML-based equalization in O-band systems have been reported to date, most of which focused on single-wavelength short-reach O-band transmission [17-19]. In

[17], an artificial NN-based equalizer was proposed for a 1310-nm 20-Gb/s 4-ary pulse amplitude modulation (PAM4) transmission over 18-km length of SMF. Significant reduction in the nonlinearity-induced penalty was demonstrated, leading to increased system capacity. The performance of a conventional NN-based equalizer was evaluated in both the C- and O-bands over 25 km of SMF, showing superior resistance to nonlinearity and noise introduced in the transmission [18]. In [19], we proposed a bidirectional gated recurrent unit (GRU) network based equalization scheme for 4×50-Gb/s O-band coarse WDM (CWDM) Nyquist on-off keying (OOK) transmission and demonstrated significant receiver sensitivity improvements in both back-to-back (B2B) and 50-km long SMF links compared to the conventional decision feedback equalizer (DFE).

In this paper, we propose to use the bidirectional Vanilla recurrent NN (Vanilla-RNN) based equalization scheme in O-band CWDM transmission. Through a 4×50-Gb/s IM/DD setup, we show that Vanilla-RNN equalization can achieve significantly better BER performance compared to the conventional DFE scheme for both Nyquist OOK and PAM4 signals. Consequently, by using Vanilla-RNN equalization, transmission of the 200-Gb/s OOK and PAM4 signals is demonstrated over 100 km and 75 km, respectively. Moreover, the performance of the Vanilla-RNN scheme regarding BER and implementation complexity is further evaluated by comparison with other linear/nonlinear schemes, including the linear equalizer, 3rd-order Volterra, and Volterra +DFE.

The rest of this paper is organized as follows: In section II, the principle of the Vanilla-RNN equalizer will be presented. Section III shows the experimental setup of the O-band CWDM IM/DD system. The experimental results of the 4×50-Gb/s O-band CWDM transmission are given in Section IV. Section V presents a comparison amongst different equalization schemes. Finally, the conclusions of this work are summarized in Section VI.

II. Principle of the Proposed ML-Assisted Equalization

The illustration of Vanilla-RNN unit employed in this work is shown in Fig. 1(a), and its output h_t is given by

$$h_t = tanh(W \cdot h_{t-1} + U \cdot x_t), \tag{1}$$

where the W and U matrices contain the weights of connections; x_t, h_t, h_{t-1} are the input, hidden output, and previous hidden output, respectively; and *tanh* denotes the hyperbolic tangent activation function.

Fig. 1(b) shows the layered diagram of the bidirectional Vanilla-RNN equalizer. Its input x is a $N \times L$ vector of the match-filtered OOK/PAM4 signal at the receiver (Rx), where N denotes the total number of input symbols, and $L = 2k + 1$ stands for the length of the input. The input x has F features (Note that features refer to individual measurable characteristics of the input, and in our work, the input symbol sequence itself is defined as the only feature, thus $F = 1$ for both OOK and PAM4). At time t, the input can be expressed as

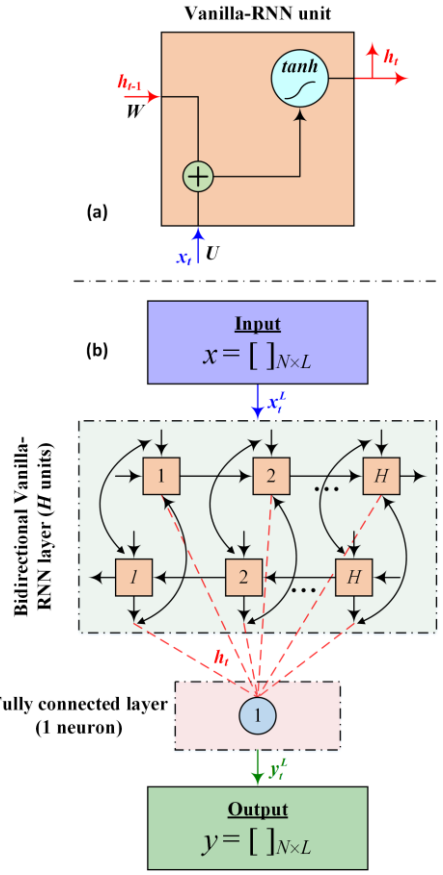

Fig. 1. (a) Conceptual illustration of the Vanilla-RNN unit, and (b) diagram of the bidirectional Vanilla-RNN equalizer.

$$x_t^L = [x_{t-k}, \ldots, x_{t-1}, x_t, x_{t+1} \ldots, x_{t+k}]. \tag{2}$$

This means that at time t, k preceding and k succeeding symbols to the current symbol x_t are used to track the inter-symbol dependencies. The extent of the length L depends on the foreseen channel memory, which relates to the accumulated CD in the SMF and the bandwidth limitation of the transceiver. Furthermore, the input was fed as a sliding window, so that the network could learn the extent of the inter-symbol interference. As shown in Fig. 1(b), the input x first goes through the bidirectional Vanilla-RNN layer with H hidden units, which will process the input in both the forward (left-to-right) and backward (right-to-left) directions. Note that double-ended arrows in Fig. 1(b) are used to indicate that the hidden units will handle both preceding and succeeding symbols (i.e., with their inputs being x_{t-k}, ...,x_{t-1}, x_t, x_{t+1}, ..., x_{t+k}), whereas the single-ended arrows mean that the hidden units will process the same input (x_t). The output of the Vanilla-RNN layer, i.e., h_t, is then sent to the fully connected layer which consists of only one neuron ($n = 1$) for both the OOK and the PAM4 cases. The fully connected layer adopts the regression approach for bit classification, which significantly reduces the implementation complexity without sacrificing the BER performance, compared to the symbol-wise classification approach [20]. The final output of the Vanilla-RNN equalizer at time t is given by

$$y_t^L = [y_{t-k}, \ldots, y_{t-1}, y_t, y_{t+1} \ldots, y_{t+k}]. \quad (3)$$

In this way, the Vanilla-RNN equalizer was trained by the *many-to-many* approach (i.e., many input symbols and many output symbols), which produces simultaneously the same number of symbols y as those at the input x [21, 22]. In this work, the length of the input word (L) was set to 21. Accordingly, the Vanilla-RNN equalizer outputs 21 equalized symbols, out of which K symbols were used for subsequent OOK/PAM4 de-mapping. As has been demonstrated in [22], the symbols at the center of the word exhibit comparable BERs and optimal performance, whilst the BER performance will gradually degrade when the symbol is away from the center of the word. Therefore, in this work, the central K = 10 symbols that share similar (and optimal) BER performance were used for de-mapping. The numbers of hidden units (H) for OOK and PAM4 were set to be 8 and 10, respectively. Note that this slightly higher number of hidden units for PAM4 was to account for its greater vulnerability to nonlinearities, owing to its higher-order nature. The Vanilla-RNN equalizer was built, trained and evaluated in *Keras* with *Tensorflow* 2.3 GPU backend. In the Keras platform, *mean square error* (MSE) and *Adam* were chosen as the loss function and optimizer for BER evaluation, respectively. For each data frame captured at the Rx, we considered 40,000 symbols for training, 20,000 symbols for validation, and 60,000 symbols for testing with unknown data, and in total five data frames were used for BER calculation. The training stage was executed with batches of 1000 words of symbols for the optimal balance between memory allocation size and execution time. At the training stage, in order to obtain the weights in Eq. (1), the back-propagation through time algorithm was used to compute the gradient, whilst the stochastic gradient descent algorithm was used to perform learning using this gradient [23]. Furthermore, all words of symbols in each batch are processed in parallel using GPUs at the training stage. While the amount of memory scales with the batch size, the advantage of multicore architectures of GPUs is normally underutilized if the batches are relatively small [23]. Therefore, we have optimized the balance between memory allocation and execution time, which resulted in the batch size of 1000 words of symbols. Note that the batch size does not affect the equalization performance, since it only adjusts the rate at which the gradients are evaluated. The maximum forward and backward passes of all training sequences (epochs) were both 500. The number of epochs, i.e., the number of complete passes through the training dataset, is related to the batch size and the length of training set. While reducing the number of epochs will result in complexity reduction of the training stage, it will also sacrifice some of the transmission performance. On the other hand, despite the training stage being a computationally demanding procedure, optical fiber channels are relatively stable over time, making it unlikely to require further re-training processes. As a result, the training complexity is not expected to affect the overall complexity of the system, as explicitly detailed in [20]. To avoid overfitting in the training stage, we adopted an '*early stopping*' process when the validation loss did not decrease after 20 successive epochs.

We note that the Vanilla-RNN model is adopted for the implementation of equalization, because it offers similar performance compared to other RNN models (e.g., long short-term memory, and gated recurrent unit) while exhibiting the lowest computational complexity [22]. A detailed comparative analysis regarding the pros and cons of the three types of RNN models can be found in [22].

III. Experimental Setup

To verify the performance of the proposed Vanilla-RNN equalizer, we implemented an O-band 4×50-Gb/s/λ CWDM system, as shown in Fig. 2(a). The transmitter (Tx) consisted of four continuous wave lasers and two Mach-Zehnder modulators (MZMs). The odd channels (1330.6 nm and 1351.1 nm) and even channels (1343.1 nm and 1360.0 nm) were fed into different MZMs for WDM channel de-correlation. In this way, the odd and even WDM channels can be fully de-correlated, and negligible impact from channel correlation is expected in our experiments. After the MZMs, the modulated optical signals were combined via an optical coupler and then amplified by a booster BDFA. The launch power to the SMF

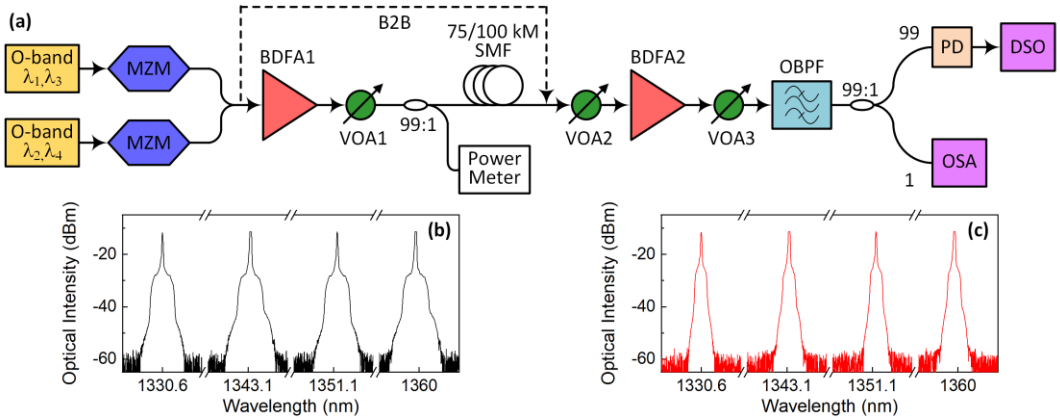

Fig. 2. (a) Experimental setup of the O-band CWDM transmission, and optical spectra of the modulated signals after the MZMs in the case of (b) Nyquist OOK and (c) Nyquist PAM4.

was controlled by a variable optical attenuator (VOA1), 1% of which was tapped out for power monitoring. After transmission in the SMF, another VOA (VOA2) was used to adjust the input power to the pre-amplifier (BDFA2), so as to vary the optical signal-to-noise ratio (OSNR) at the Rx. Following BDFA2, another VOA (VOA3) was used to ensure that a constant optical power (around -10 dBm) was fed to the photodetector (PD, *Finisar XPRV2022A*) in all OSNR cases and for all WDM channels. Note that the PD offered a typical conversion gain of 500 V/W thanks to the integration of a trans-impedance amplifier, which ensured that the received optical power used in the experiments was well above the sensitivity limit of the PD. An optical bandpass filter (OBPF) with a bandwidth of 1.2 nm was used to select the WDM channel for performance evaluation. 1% of the optical signal after the OBPF was fed into an optical spectrum analyzer (OSA) for OSNR monitoring at 0.1-nm resolution bandwidth. Note that similar to the prior works [24, 25], the measurement of the signal power in the OSNR calculations accounted for both the optical carrier and the sideband signal. It is worth noting that the CWDM settings in this work (i.e., ~1330 to 1360 nm with a 10-nm spacing) are mainly chosen to suit the gain profile of the used BDFAs. While this experimental choice might not be in accordance to recent standards (e.g., 200GBASE-FR4), our experiments offer a useful exploration of the performance of ML-assisted equalization in reach-extended O-band WDM systems.

Thanks to the use of optical amplification, the lengths of SMF adopted in the CWDM experiments were up to 75 km and 100 km for the Nyquist PAM4 and Nyquist OOK transmission, respectively. The insertion losses of the 75-km and 100-km SMFs were around 23.5 dB and 31.3 dB, respectively, at the wavelengths of interest. The CD values of the SMF at the four WDM wavelengths were estimated to be 1.5, 2.3, 3.3, and 3.8 ps/nm/km, respectively. The booster BDFA1 had a gain of ~20 dB at an input power of -6 dBm, and the pre-amplifier BDFA2 exhibited >25-dB gain under -20-dBm input power. We also evaluated the performance of the system in the back-to-back (B2B) case, wherein the booster BDFA1 and transmission fiber were excluded, as indicated by the dashed line in Fig. 2(a). The optical spectra of the 4×50-Gb/s/λ WDM signals in the Nyquist OOK transmission and Nyquist PAM4 transmission cases are shown in Fig. 2(b) and Fig. 2(c), respectively.

Despite the CD values being relatively low at the four WDM wavelengths, the impact of CD is cumulative with transmission distance. This means that when the length of the fiber link is sufficiently long, CD will eventually cause destructive power fading for O-band transmission, resulting in severe inter-symbol interference. Using these values, we have simulated the CD-induced power fading for the four CWDM channels after 75-km and 100-km SMF transmission, and the results are presented in Fig. 3. It is clearly seen that severe power fading will be experienced, especially at longer wavelength (i.e., more dispersive) channels. This indicates that efficient equalization techniques which can effectively combat the power fading (and thus inter-symbol interference), such as those studied in this work, are highly desirable for reach-extended O-band WDM transmission.

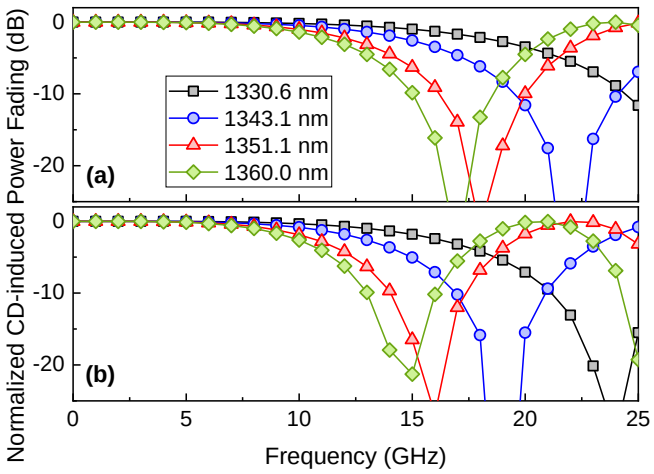

Fig. 3. Numerical results of the CD-induced power fading at the four O-band CWDM channels after (a) 75-km and (b) 100-km SMF transmission.

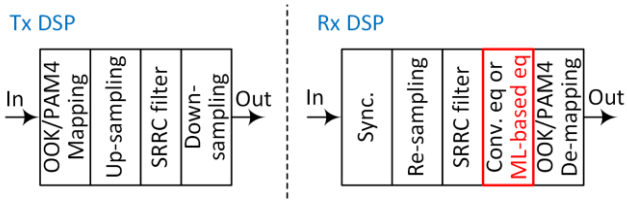

Fig. 4. DSP blocks for the Nyquist OOK/PAM4 signals.

The Nyquist OOK and Nyquist PAM4 signals were generated and processed offline using the digital signal processing (DSP) blocks shown in Fig. 4. At the Tx, the binary input was first mapped to either OOK or PAM4 symbols, followed by 90-times up-sampling and square-root raised cosine (SRRC) filtering. The SRRC filter used a roll-off factor of 0.1 and a span of 40 symbols. The pseudorandom unrepeated binary input was generated by using rng('shuffle') and the Mersenne Twister generator with a period of 2^{19937}-1. The filtered signal was then 50-times and 25-times down-sampled in the OOK and PAM4 cases, respectively. Finally, the resulting signal was fed into a 90-GSa/s arbitrary waveform generator (AWG) for the generation of the 50-Gb/s Nyquist OOK/PAM4 signal. We note that for simplicity, 90-times up-sampling was used to match the sampling rate of the AWG (90 GSa/s). To generate 50-Gb/s signals, the up-/down-sampling factors can be reduced as long as the ratios between them are equal to 18/5 and 9/5 for PAM4 and OOK, respectively. At the Rx, the captured data from the digital storage oscilloscope (DSO) were first synchronized and re-sampled before matched SRRC filtering was applied. Subsequently, either a conventional equalization scheme or the proposed Vanilla-RNN equalizer was applied to the filtered signal before performing OOK/PAM4 de-mapping. After de-mapping, the recovered binary sequence was used to calculate the BER of the transmission via error counting.

We note that the conventional DFE equalizer, which can deal with the CD-induced power fading [26] in longer-reach O-band CWDM systems, was first used as a benchmark to evaluate the performance of our proposed Vanilla-RNN equalization scheme. The DFE equalizer was half-symbol-spaced (i.e., the

input was re-sampled at 2 samples/symbol) and the recursive least squares (RLS) adaptive algorithm was adopted in the DFE scheme, and the numbers of feedforward and feedback taps were optimized to be 17 and 7, respectively. We note that the DFE equalizer was operated at 2 samples/symbol to offer better performance, as this can combat the aliasing issue and is less sensitive to phase sampling delay [27]. In contrast, the Vanilla-RNN equalizer was only symbol-spaced to reduce implementation complexity, yet this can still offer excellent BER performance as will be demonstrated in the following. In Section V, we present results where the 1330.6-nm channel is used as an example to perform a more comprehensive comparison that also includes the linear equalizer (i.e., FFE), Volterra and Volterra+DFE schemes.

IV. Experimental Results of the O-band CWDM Transmission

A. *B2B transmission*

The performance of the Vanilla-RNN equalizer was first characterized in the B2B link of the O-band CWDM system and the results for OOK and PAM4 are shown in Fig. 5 and Fig. 6, respectively. Note that the dashed lines shown in the figures represent the corresponding linear fitting results. It is seen that in both OOK and PAM4 cases, the four WDM channels exhibited comparable BER versus OSNR performance. For the 50-Gb/s/λ Nyquist OOK B2B transmission shown in Fig. 5, BERs below the hard decision forward error correction limit (HD-FEC, 3.8×10^{-3}) were achieved. Meanwhile, compared to the conventional DFE scheme, the proposed Vanilla-RNN equalization required around 1 dB lower OSNR to realize BERs below the HD-FEC limit.

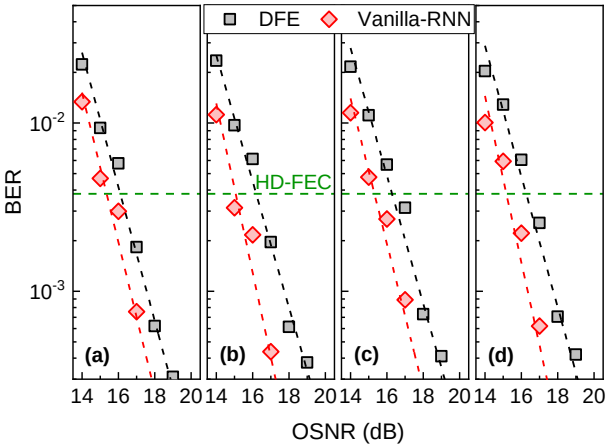

Fig. 5. BER versus OSNR for the B2B Nyquist OOK transmission at: (a) 1330.6 nm, (b) 1343.1 nm, (c) 1351.1 nm, and (d) 1360.0 nm. Dashed lines: results of linear fitting.

In comparison, as shown in Fig. 6, for 50-Gb/s/λ Nyquist PAM4 transmission, the Vanilla-RNN scheme offered ~2-dB OSNR sensitivity enhancements at the HD-FEC limit. The more significant improvements in the PAM4 transmission case are attributed to the fact that PAM4 is more susceptible to system nonlinearities [16] originating from the transceivers, as compared to OOK.

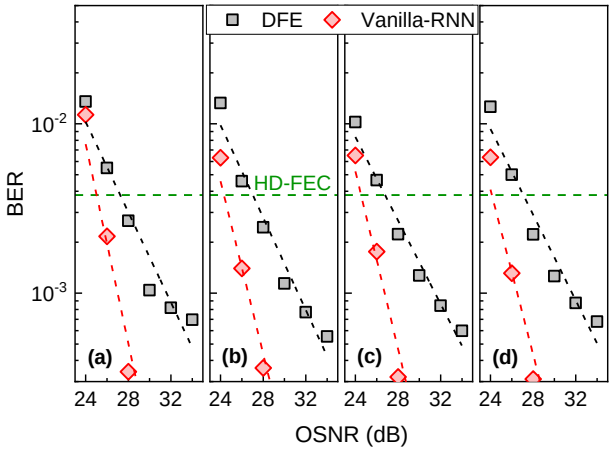

Fig. 6. BER versus OSNR for the B2B Nyquist PAM4 transmission at: (a) 1330.6 nm, (b) 1343.1 nm, (c) 1351.1 nm, and (d) 1360.0 nm. Dashed lines: results of linear fitting.

B. *100-km OOK transmission and 75-km PAM4 transmission*

We next carried out transmission experiments of the 50-Gb/s/λ OOK and PAM4 CWDM signals over 100-km and 75-km lengths of SMF, respectively. The 1330.6-nm channel was taken as an example to investigate the BER performance versus total launch power and the corresponding results are presented in Fig. 7 for both the OOK and the PAM4 cases.

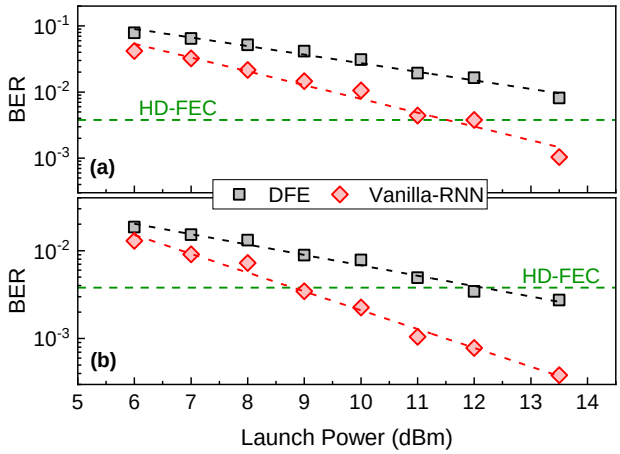

Fig. 7. BER versus total launch power of the 1330.6-nm channel: (a) Nyquist OOK transmission after 100-km length of SMF, and (b) Nyquist PAM4 transmission after 75-km length of SMF. Dashed lines: results of linear fitting.

It is seen that in both cases, the BER was reduced with an increase in the total launch power, and no performance degradation was observed under a launch power as high as 13.5 dBm (i.e., ~7.5 dBm/channel). This was mainly due to the coarsely spaced WDM channels (~10-nm spacing), which offered enhanced tolerance to fiber nonlinearity. As shown in Fig. 7(a), the lowest BER achieved when using the DFE scheme in 50-Gb/s 1330.6-nm 100-km Nyquist OOK transmission was still above the HD-FEC, even when the maximum available total launch power of 13.5 dBm was used. When using the Vanilla-RNN equalization, BERs below the HD-FEC limit could be achieved. To obtain the same BER as with the DFE scheme, a launch power reduced by ~2.5 dB was

required. For 75-km Nyquist PAM4 transmission, the DFE scheme was able to realize BERs slightly below the HD-FEC limit. However, as shown in Fig. 7(b), significantly lower BERs could be achieved for the same launch power when adopting the Vanilla-RNN equalizer. Approximately 3-dB lower launch power was required to achieve a BER below the HD-FEC limit when Vanilla-RNN was adopted.

With a fixed launch power of 13.5 dBm, we then investigated the BER performance of both 100-km OOK and 75-km PAM4 transmission under different OSNRs at the four WDM channels. Fig. 8 shows the results in the 100-km OOK transmission case.

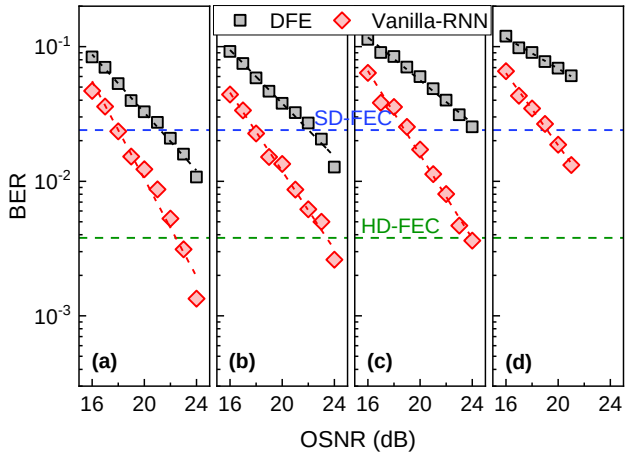

Fig. 8. BER versus OSNR for the Nyquist OOK transmission after 100-km length of SMF: (a) 1330.6 nm, (b) 1343.1 nm, (c) 1351.1 nm, and (d) 1360.0 nm. Dashed lines: results of linear fitting.

It is seen that the BER performance degraded with an increase in wavelength. This resulted from the increased CD at longer wavelengths [16], which imposed a more severe CD-induced power fading. As a result, none of the four channels were able to achieve a BER lower than the HD-FEC limit when using the DFE scheme. Even when the soft decision FEC (SD-FEC, 2.4×10^{-2}) limit was considered, only the shortest two wavelengths (i.e., 1330.6 nm and 1343.1 nm) could achieve BERs below this limit. By using the Vanilla-RNN equalizer instead, the BERs of all four channels were well below the SD-FEC limit, which corresponded to at least 4-dB OSNR sensitivity improvement. In addition, the BER performance amongst the four channels exhibited minor differences when compared to that in the DFE case. This indicates that the Vanilla-RNN equalization is almost wavelength agnostic, proving its ability to compensate for the CD-induced power fading effect. Nevertheless, further BER performance improvements can be achieved in longer wavelength (i.e., more dispersive) channels through the use of a larger number of hidden units and/or a longer word length. However, this will inevitably result in an increase in the implementation complexity of the Vanilla-RNN scheme. Note that although substantial BER reduction was demonstrated at the 1360.0-nm channel relative to the DFE scheme, the achievable BER performance was restricted by the available OSNR, which was due to the lower gain of the BDFAs at this wavelength.

Compared to the Nyquist OOK, Nyquist PAM4 occupies half the signal bandwidth while realizing the same data rate, though this comes at the expense of an increased susceptibility to nonlinear distortions. The halved bandwidth, however, provides four times higher tolerance to the CD-induced power fading. As a result, similar BER performance could be achieved for the first three WDM channels in the 75-km PAM4 transmission case, and the longest-wavelength channel only exhibited minor BER performance degradation. As shown in Fig. 9, the Vanilla-RNN equalization offered around 1-dB and 4-dB OSNR sensitivity improvements at the SD-FEC and HD-FEC limits, respectively. Similar to the OOK case, the achievable BER of the 1360.0-nm channel was also compromised by the available OSNR due to the lower gain of the BDFAs at this channel.

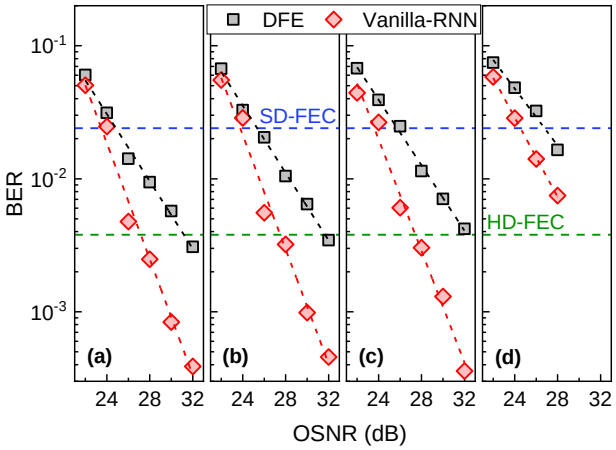

Fig. 9. BER versus OSNR for the Nyquist PAM4 transmission after 75-km length of SMF: (a) 1330.6 nm, (b) 1343.1 nm, (c) 1351.1 nm, and (d) 1360.0 nm. Dashed lines: results of linear fitting.

By comparing the results of the OOK transmission for B2B and the 100-km SMF link, it is clear that the proposed Vanilla-RNN equalization offers significantly better tolerance to the CD-induced power fading, compared to the DFE scheme. In addition, for the PAM4 transmission, the OSNR sensitivity improvement increased from ~2 dB in the B2B to ~4 dB after fiber transmission, thereby confirming that the Vanilla-RNN scheme also exhibits superior capability to combat impairments in the transmission fiber.

V. Performance Comparison Amongst Different Equalization Schemes

In this section, we present one further evaluation study of the performance of Vanilla-RNN equalization by comparing it with a few other existing linear/nonlinear equalization schemes. In addition to DFE which was already presented above, these include the linear equalizer, nonlinearVolterra and nonlinear Volterra+DFE schemes. Unlike the DFE scheme, the linear equalizer is less effective in terms of combating the frequency-selective fading, but it has lower implementation complexity [6, 28]. On the other hand, it has been demonstrated that nonlinear Volterra equalization is very effective against the

nonlinearities of both the transceivers and the transmission fiber, although its complexity is also substantially higher than that of the linear/DFE schemes [28]. We have also included the scheme of Volterra+DFE, in which DFE is cascaded after the Volterra equalizer to enhance its ability to tackle power fading.

For the linear equalizer, the number of taps was 25, and it used the same adaptive RLS algorithm as was adopted in the DFE scheme. The order of the nonlinear Volterra was 3, and the corresponding tap numbers were 21, 11, and 5, respectively. To ensure a fair comparison amongst the different equalizers, these respective numbers of taps were optimized to achieve the optimal BER performance at a relatively low computational complexity. We take the 1330.6 nm channel as an example to investigate their respective BER performance versus OSNR in both B2B and 100/75-km SMF links for Nyquist OOK/PAM4 signals. The analysis with regard to the implementation complexity will be also presented.

A. BER comparisons

Fig. 10 shows the BER results of different equalization schemes in the B2B OOK case. It is seen that the DFE, Volterra, and Volterra+DFE schemes showed comparable BER performance, which was slightly better than that achieved by the linear equalizer. The proposed Vanilla-RNN equalizer exhibited the best BER performance amongst these schemes, and the required OSNR to achieve a BER below the HD-FEC limit was reduced by ~0.5 dB.

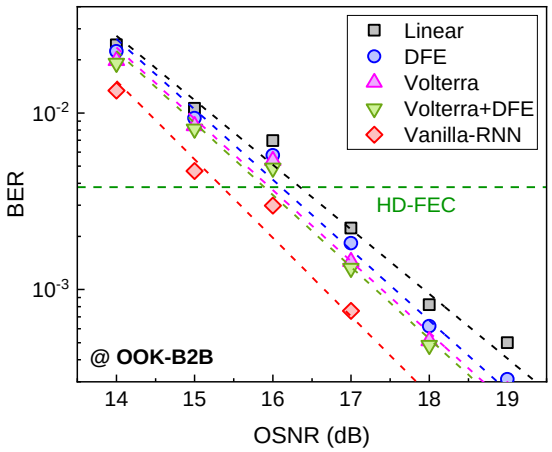

Fig. 10. BER versus OSNR of different equalization schemes in the B2B Nyquist OOK transmission at the 1330.6-nm channel. Dashed lines: results of linear fitting.

In comparison, as shown in Fig. 11, when the higher-order PAM4 format was used, the linear and DFE schemes showed almost the same BER performance, indicating that the DFE scheme is also less effective against transceiver nonlinearities. When using the Volterra scheme, a considerable BER reduction was achieved, showing that the Volterra equalizer is capable of compensating for the nonlinearities of components in the B2B link. Cascading an additional DFE after the Volterra (i.e., Volterra+DFE) did not introduce much performance improvement, since no power fading was experienced in the PAM4 B2B link. Furthermore, once again Fig. 11 confirms that the optimal BER performance was still achieved by the Vanilla-RNN scheme. While the Volterra, Volterra+DFE, and Vanilla-RNN schemes could all achieve BERs lower than that of the linear/DFE scheme, the Vanilla-RNN scheme exhibited the best OSNR sensitivity.

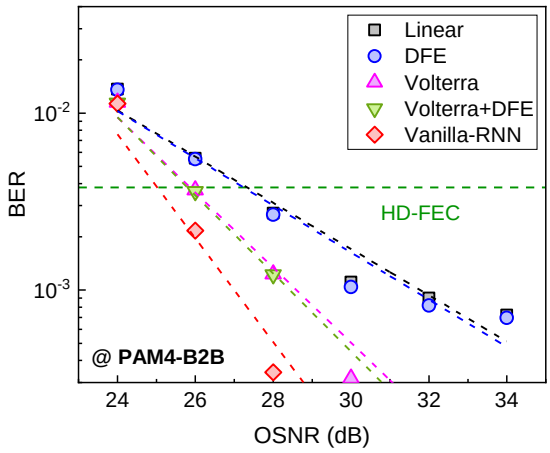

Fig. 11. BER versus OSNR of different equalization schemes in the B2B Nyquist PAM4 transmission at the 1330.6-nm channel. Dashed lines: results of linear fitting.

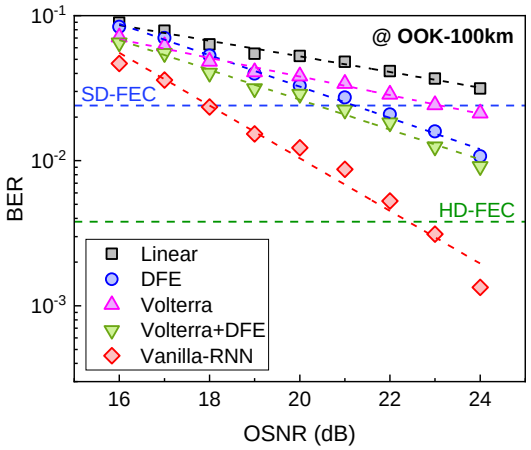

Fig. 12. BER versus OSNR of different equalization schemes in the Nyquist OOK transmission at the 1330.6-nm channel after 100-km length of SMF. Dashed lines: results of linear fitting.

We then investigated the performance of these equalization schemes when the signals were transmitted in 100/75-km lengths of SMF for Nyquist OOK/PAM4. The results of the 100-km OOK transmission are presented in Fig. 12. Similar to the B2B case, the linear equalizer showed the worst BER performance. On the other hand, since the Volterra scheme cannot combat the CD-induced power fading, its BER performance was worse than that of the DFE and Volterra+DFE schemes. In this case, the inclusion of DFE after the 3rd-order Volterra equalizer was beneficial as it could further mitigate the impact of CD-induced power fading, thus improving the BER performance. However, none of these conventional schemes could achieve a BER below the HD-FEC limit at the highest OSNR of 24 dB. In contrast, by using the Vanilla-RNN scheme, a BER well below the HD-FEC limit was demonstrated.

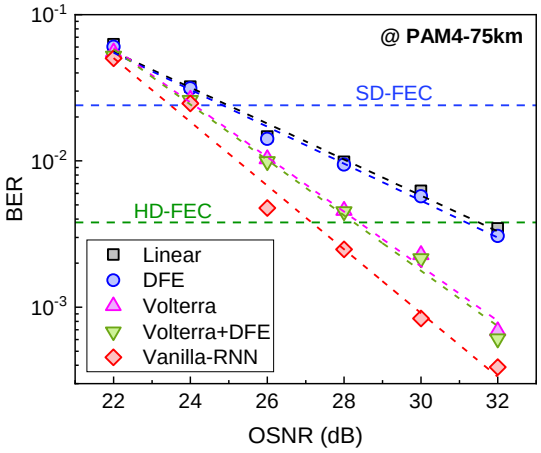

Fig. 13. BER versus OSNR of different equalization schemes in the Nyquist PAM4 transmission at the 1330.6-nm channel after 75-km length of SMF. Dashed lines: results of linear fitting.

Unlike the 100-km OOK transmission case wherein the CD-induced power fading dominated the BER performance, as we have mentioned in Section IV.B, after transmission in the 75-km length of SMF, the CD-induced power fading effect for the 1330.6-nm channel was still relatively minor. Instead, the nonlinearities originating from both the components and the SMF determined the performance of the PAM4 transmission. As a result, the BER performance of different equalization schemes behaved in a similar manner to that in the B2B PAM4 link shown in Fig. 11. The linear and DFE schemes exhibited comparable BER versus OSNR performance, and both of them required ~3-dB higher OSNR to realize a BER lower than the HD-FEC limit, when compared to the Volterra/Volterra+DFE approach. Furthermore, the use of the Vanilla-RNN scheme achieved the lowest BER and offered around 1-dB additional OSNR sensitivity improvement compared to the Volterra-based schemes, as shown in Fig. 13.

B. Comparisons of the implementation complexity

Finally, we compare the implementation complexity of different equalization schemes. We note that a comparison of the computational complexity amongst the linear, DFE and Volterra schemes has already been reported in the literature [6, 28]. For the linear/DFE scheme, the required number of real multiplications per symbol is only $N_{sample}\times N_{Tap}$, where N_{sample} is the number of samples per symbol and N_{Tap} is the total number of feedforward (and feedback) taps. Since it is known that the Volterra approach is significantly more complex than the linear and DFE schemes, in this section, we focus on a comparison between the half-symbol-spaced 3rd-order Volterra-based equalizer and the symbol-spaced Vanilla-RNN.

While the computation of the *tanh*(*) function in the Vanilla-RNN is relatively complex, the FPGA implementations of non-linear activation functions with minor approximations and small hardware footprint (only few LUTs) [29] indicate that it can be implemented efficiently. Therefore, it is anticipated that the implementation of real multiplications represents the dominant contributor to the overall complexity. Hence, we focus on the comparison of implementation complexity in terms of the required number of real multiplications per symbol [22, 30, 31].

The complexity of the Vanilla-RNN equalizer depends on the number of features of its input (F = 1, as mentioned in Section II), the number of hidden units (H, 8 for OOK and 10 for PAM4), the length of the input word (L = 21), the number of neurons used in the fully connected layer (n = 1), and the number of simultaneously equalized symbols at its output (K = 10). The number of real multiplications per symbol to implement the *many-to-many* Vanilla-RNN scheme is given by

$$N_{Vanilla} = \frac{2(FH + H^2)L + 2HnL}{K}. \quad (4)$$

Therefore, it can be easily calculated that the required numbers of real multiplications to implement the proposed Vanilla-RNN equalizer for OOK and PAM4 signals are 336 and 504, respectively.

In contrast, the required number of real multiplications per OOK/PAM4 symbol for the implementation of the half-symbol-spaced 3rd-order Volterra equalizer is given as [22, 30],

$$N_{Volterra} = 2\times\sum_{j=1}^{3}\frac{(L_j - 1 + j)!}{(j-1)!\,(L_j - 1)!}. \quad (5)$$

where (·)! denotes the factorial operation; L_1 = 21, L_2 = 11, and L_3 = 5 are the numbers of taps of the 3rd-order Volterra equalizer. It can then be calculated that $N_{Volterra}$ = 516 for both the OOK case and the PAM4 case. This is greater than that needed by the Vanilla-RNN equalizer in both the OOK (i.e., 336) and the PAM4 cases (i.e., 504), as summarized in Table I. For reference, the case of the DFE scheme is also included. Despite its significantly lower required numbers of real multiplications, as clearly demonstrated in the previous sections, the corresponding transmission performance has been inferior, and cannot satisfy the reach-extended O-band CWDM transmission.

TABLE I
COMPARISON OF THE REQUIRED NUMBERS OF REAL MULTIPLICATIONS

	DFE	Volterra	Vanilla-RNN
OOK	48	516	336
PAM4	48	516	504

It is also worth noting that previous work carried out using dense WDM (DWDM) coherent signals in the C-band suggests that Vanilla-RNN is also well-suited to the processing of DWDM channels [20, 22]. On the other hand, if the scheme is to be applied to IM/DD signals in the C-band, it is anticipated that a larger number of hidden units and/or a longer word length will be necessary to combat the higher CD of the fiber in order to achieve acceptable transmission performance, which however will increase the implementation complexity.

VI. CONCLUSION

In this paper, we have proposed and demonstrated the use of a bidirectional Vanilla-RNN equalizer for 50-Gb/s/λ O-band

CWDM IM/DD transmission. By applying the Vanilla-RNN equalization to Nyquist OOK/PAM4 over both B2B and 100/75-km long SMF links, it was demonstrated that the Vanilla-RNN equalizer is capable of compensating for both transceiver nonlinearity as well as the CD and nonlinearity in SMF. We also showed that Vanilla-RNN equalization exhibits significantly better BER performance than the conventional DFE scheme. This enabled 4×50-Gb/s Nyquist OOK and PAM4 transmission over up to 100-km and 75-km lengths of SMF, respectively. Furthermore, through a comparison amongst the linear, DFE, Volterra and Volterra+DFE schemes, we demonstrated that Vanilla-RNN achieved the best BER performance. Additionally, its implementation complexity is also lower than that of the Volterra-based schemes, highlighting the potential for its use in practical longer-reach O-band CWDM systems.

ACKNOWLEDGMENT

Y. Hong would like to acknowledge Dr. Zhouyi Hu at Aston University, United Kingdom for his help with the Volterra equalization. The data for this work is accessible through the University of Southampton Institutional Research Repository (DOI: https://doi.org/10.5258/SOTON/D2140).

REFERENCES

[1] D. Zibar, H. Wymeersch, and I. Lyubomirsky, "Machine Learning Under the Spotlight," *Nat. Photon*., vol. 11, pp. 749-751, 2017.
[2] D. Zibar, M. Piels, R. Jones, *et al*., "Machine Learning Techniques in Optical Communication," *J. Lightw. Technol.*, vol. 34, no. 6, pp. 1442-1452, 2016.
[3] F. Musumeci, C. Rottondi, A. Nag, *et al*., "An Overview on Application of Machine Learning Techniques in Optical Networks," *J. Lightw. Technol.*, vol. 21, no. 2, pp. 1383-1408, 2019.
[4] F.N. Khan, Q. Fan, C. Lu, *et al*., "An Optical Communication's Perspective on Machine Learning and Its Applications," *J. Lightw. Technol*., vol. 37, no. 2, pp. 493-516, 2019.
[5] S. Gaiarin, X. Pang, O. Ozolins, *et al*., "High Speed PAM-8 Optical Interconnects with Digital Equalization based on Neural Network," in *Proc. of ACP*, Wuhan, China, paper AS1C.1, 2016.
[6] H. Zhou, Y. Li, Y. Liu, *et al*., "Recent Advances in Equalization Technologies for Short-Reach Optical Links Based on PAM4 Modulation: A Review," *Appl. Sci*., vol. 9, no. 11, 2342, 2019.
[7] K. Zhong, X. Zhou, J. Huo, *et al*., "Digital Signal Processing for Short-Reach Optical Communications: A Review of Current Technologies and Future Trends," *J. Lightw. Technol*., vol. 36, no. 2, pp. 377-400, 2018.
[8] B. Karanov, M. Chagnon, F. Thouin, *et al*., "End-to-End Deep Learning of Optical Fiber Communications," *J. Lightw. Technol*., vol. 36, no. 20, pp. 4843-4855, 2018.
[9] L. Yi, T. Liao, L. Huang, *et al*., "Machine Learning for 100 Gb/s/λ Passive Optical Network," *J. Lightw. Technol*., vol. 37, no. 6, pp. 1621-1630, 2019.
[10] J. He, J. Lee, T. Song, *et al*., "Recurrent Neural Network (RNN) for Delay-tolerant Repetition-coded (RC) Indoor Optical Wireless Communication Systems," *Opt. Lett*., vol. 44, no. 15, pp. 3745-3748, 2019.
[11] B. Karanov, D. Lavery, P. Bayvel, *et al*, "End-to-end Optimized Transmission over Dispersive Intensity-modulated Channels using Bidirectional Recurrent Neural Networks," *Opt. Express*, vol. 27, no. 14, pp. 19650-19663, 2019.
[12] N. Taengnoi, K.R.H. Bottrill, N.K. Thipparapu, *et al*., "WDM Transmission With In-Line Amplification at 1.3μm Using a Bi-Doped Fiber Amplifier," *J. Lightw. Technol.*, vol. 37, no. 8, pp. 1826-1830, 2019.
[13] N. Taengnoi, K.R.H. Bottrill, Y. Hong, *et al*., "4-Level Alternate-Mark-Inversion for Reach Extension in the O-Band Spectral Region," *J. Lightw. Technol.*, vol. 39, no. 9, pp. 2847-2853, 2021.
[14] E.M. Dianov, "Amplification in Extended Transmission Bands Using Bismuth-Doped Optical Fibers," *J. Lightw. Technol*., vol. 31, no. 4, pp. 681-688, 2013.
[15] N. K. Thipparapu, A. A. Umnikov, P. Barua, *et al*., "Bi-doped fiber amplifier with a flat gain of 25 dB operating in the wavelength band 1320–1360 nm," *Opt. Lett*., vol. 41, no. 7, pp. 1518-1521, 2016.
[16] Y. Hong, K.R.H. Bottrill, N. Taengnoi, *et al*., "Numerical and Experimental Study on the Impact of Chromatic Dispersion on O-band Direct-detection Transmission," *Appl. Opt*., vol. 60, no. 15, pp. 4383-4390, 2021.
[17] A.G. Reza, and J.K.K. Rhee, "Nonlinear Equalizer Based on Neural Networks for PAM-4 Signal Transmission Using DML," *IEEE Photon. Technol. Lett*., vol. 30, no. 15, pp. 1416-1419, 2018.
[18] P. Li, L. Yi, L. Xue, *et al*., "100Gbps IM/DD Transmission over 25km SSMF using 20G-class DML and PIN Enabled by Machine Learning," in *Proc. of OFC*, San Diego, USA, paper W2A.46, 2018.
[19] Y. Hong, S. Deligiannidis, N. Taengnoi, *et al*., "Performance-enhanced Amplified O-band WDM Transmission using Machine Learning based Equalization," in *Proc. of CLEO*, San Jose, USA, paper STh1F.3, 2021.
[20] S. Deligiannidis, A. Bogris, C. Mesaritakis, *et al*., "Compensation of Fiber Nonlinearities in Digital Coherent Systems Leveraging Long Short-term Memory Neural Networks," *J. Lightw. Technol*., vol. 38, no. 21, pp. 5991-5999, 2020.
[21] I. Sutskever, O. Vinyals, and Q.V. Le, "Sequence to sequence learning with neural networks," in *Proc. of NIPS*, Montreal, Canada, pp. 1-9, 2014.
[22] S. Deligiannidis, C. Mesaritakis, and A. Bogris, "Performance and Complexity Analysis of Bi-directional Recurrent Neural Network Models vs. Volterra Nonlinear Equalizers in Digital Coherent Systems," *J. Lightw. Technol*., vol. 39, no. 18, pp. 5791-5798, 2021.
[23] I. Goodfellow, Y. Bengio, and A. Courville, "Deep Learning," *MIT press*, 2016.
[24] Y. Zhu, K. Zou, Z. Chen, *et al*., "224 Gb/s Optical Carrier-Assisted Nyquist 16-QAM Half-Cycle Single-Sideband Direct Detection Transmission over 160 km SSMF," *J. Lightw. Technol*., vol. 35, no. 9, pp. 1557-1565, 2017.
[25] Z. Li, M.S. Erkılınc, K. Shi, *et al*., "SSBI Mitigation and the Kramers–Kronig Scheme in Single-Sideband Direct-Detection Transmission With Receiver-Based Electronic Dispersion Compensation," *J. Lightw. Technol*., vol. 35, no. 10, pp. 1887-1893, 2017.
[26] R. Rath, D. Clausen, S. Ohlendorf, *et al*., "Tomlinson–Harashima Precoding For Dispersion Uncompensated PAM-4 Transmission With Direct-Detection," *J. Lightw. Technol*., vol. 35, no. 18, pp. 3909-3917, 2017.
[27] M.D. Santa, C. Antony, G. Talli, *et al*., "25Gb/s PAM4 Adaptive Receiver Equalisation Requirements for Burst-Mode Transmission Systems," in *Proc. of ECOC*, Düsseldorf, Germany, pp. 424-426, 2016.
[28] G.W. Lu, H.B. Zhang, S. Shinada, *et al*., "Power-Efficient O-Band 40 Gbit/s PAM4 Transmitter Based on Dual-Drive Cascaded Carrier-Depletion and Carrier-Injection Silicon Mach-Zehnder Modulator With Binary Driving Electronics at CMOS Voltages," *IEEE J. Sel. Top. Quantum. Electron*., vol. 27, no. 3, paper 3500308, 2021.
[29] A.M. Abdelsalam, J.M.P. Langlois, and F. Cheriet, "A Configurable FPGA Implementation of the Tanh Function Using DCT Interpolation," in *Proc. of FCCM*, pp. 168-171, 2017.
[30] N.P. Diamantopoulos, H. Nishi, W. Kobayashi, *et al*., "On the Complexity Reduction of the Second-Order Volterra Nonlinear Equalizer for IM/DD Systems," *J. Lightw. Technol*., vol. 37, no. 4, pp. 1214-1224, 2019.
[31] J. Tsimbinos, and K.V. Lever, "Computational Complexity of Volterra based Nonlinear Compensators," *Electron. Lett*., vol. 32, no. 9, pp. 852-854, 1996.

Yang Hong received the Ph.D. degree from The Chinese University of Hong Kong, Hong Kong, in 2018. In September 2018, he joined the Optoelectronics Research Centre at the University of Southampton as a Research Fellow and was

promoted to Senior Research Fellow in January 2022. He was a Visiting Researcher with the Department of Electrical and Electronic Engineering, The University of Melbourne, from December 2017 to May 2018. His research interests include optical wireless communications and networking, advanced signal processing, high-speed optical fibre transmission, and ultra-wideband transmission.

Stavros Deligiannidis received the B.Sc. degree in physics, the M.Sc. degree in microelectronics, and the VLSI from the National and Kapodistrian University of Athens, Athens, Greece. He is currently working toward the Ph.D. degree with the University of West Attica, Egaleo, Greece, in the field of novel signal processing techniques for optical communication systems under the supervision of Prof.Adonis Bogris. From 2010 to 2019, he was with the Department of Computer Engineering, Technological Educational Institute of Peloponesse, Antikalamos, Greece, where he served as a Lecturer. He has been involved in numerous national and European research projects in the field of optical communications and photonics. His current research interests include optical communications, deep learning, digital signal processing, and parallel computing.

Natsupa Taengnoi is currently pursuing the Ph.D. degree at the Optoelectronics Research Centre, University of Southampton. Her research interests include high-speed O-band transmission, characterization of fibre amplifiers, and digital signal processing for nonlinearity mitigation.

Kyle R. H. Bottrill received the Ph.D. degree from the Optoelectronics Research Centre, University of Southampton, in 2016, after which he continued to work as a Research Fellow. His research interests include optical signal processing, nonlinear optics, optical wavelength conversion, and high-speed optical communications.

Naresh K. Thipparapu received the Ph.D. degree in optoelectronics from the University of Southampton, Southampton, U.K. in 2018, where he is currently working as a Research Fellow. His research interests include (among others) fibre lasers and amplifiers, non-linear fibre optics, fibre design and fabrication, fibre spectroscopy, and optical materials. He is a member of Optical Society of America.

Yu Wang joined the Optoelectronics Research Centre (ORC), University of Southampton in 2018 to pursue a Ph.D. in development and application of broadband bismuth doped fibre devices. Her research interests include fibre amplifiers, fibre spectroscopy, fibre design, and fabrication. She was the recipient of the Prof. Sir David Payne Student Scholar Award in 2019 and of the Highest Performing Ph.D. Students at the ORC in the first year of their studies. She is a member of the Optical Society of America.

Jayanta K. Sahu received the M.Sc. degree in physics and the Ph.D. degree from the Indian Institute of Technology (IIT) Kharagpur, Kharagpur, India. After working with the Royal Institute of Technology, Stockholm, Sweden as a Postdoctoral Research Fellow from 1997 to 2000, he was the Optoelectronics Research Centre (ORC), University of Southampton, Southampton, U.K., where he is currently a Professor and leading the Fibre Fabrication Group. He has authored or coauthored more than 400 articles in scientific journals and conference proceedings, including many invited and post-deadline papers. Prof Sahu's research interest focuses on the optical fibre technology, in particular, optical materials, specialty optical fibres, and high-power fibre lasers, and amplifiers. He is a Senior Member of the Optical Society of America and a Fellow of Optical Society of India.

David J. Richardson received the B.Sc. and Ph.D. degrees in fundamental physics from Sussex University, Brighton, U.K., in 1985 and 1989 respectively. He joined the Optoelectronics Research Centre (ORC), University of Southampton, U.K., in 1989 and was awarded a Royal Society University Fellowship in 1991 in recognition of his pioneering work on short pulse fiber lasers. He has been the Deputy Director at ORC with responsibility of optical fibre and laser related research since 2000. He is a prominent figure in the international photonics community and has published more than 500 journal papers and produced more than 20 patents. His current research interests include amongst others: optical fiber communications, hollow core optical fibers, optical fiber amplifiers, and pulsed high-power fibre lasers. Professor Richardson was elected Fellow of the Royal Academy of Engineering in 2009 and most recently as Fellow of the Royal Society in 2018. He is also a Fellow of the IEEE, OSA and IET.

Charis Mesaritakis received the B.S. degree in informatics from the Department of Informatics and Telecommunications, National and Kapodistrian University of Athens, Athens, Greece, in 2004, the M.Sc. degree in microelectronics from the National and Kapodistrian University of Athens, and the Ph.D. degree in 2011, in the field of quantum dot devices and systems for next generation optical networks from the Photonics Technology and Optical Communication Laboratory, National and Kapodistrian University of Athens. He has actively participated as a Research Engineer or Technical Supervisor in more than ten EU-funded research programs (FP6-FP7-H2020) targeting excellence in the field of broadband communications, cyber-physical security, and photonic integration. He is currently an Associate Professor with the Department of Information and Communication Systems Engineering, University of the Aegean, Mytilene, Greece. He is the author and co-author of more than 60 papers in highly cited peer reviewed international journals and conferences, two international book chapters, whereas he is a regular Reviewer for IEEE, OSA, AIP, and Springer. In 2012, he was awarded a European Scholarship for post-doctoral studies (Marie Curie FP7-PEOPLE IEF) in the joint research facilities of Alcatel-Thales-Lucent in Paris-France, where he worked on intra-satellite communications.

Adonis Bogris (Senior Member, OSA) was born in Athens, Greece. He received the B.S. degree in informatics, the M.Sc. degree in telecommunications, and the Ph.D. degree from the National and Kapodistrian University of Athens, Athens, Greece, in 1997, 1999, and 2005, respectively. His doctoral thesis was on all-optical processing by means of fiber-based

devices. He is currently a Professor with the Department of Informatics and Computer Engineering, University of West Attica, Egaleo, Greece. He has authored or coauthored more than 150 articles published in international scientific journals and conference proceedings and he has participated in plethora of EU and national research projects. His current research interests include high-speed all-optical transmission systems and networks, nonlinear effects in optical fibers, all-optical signal processing and all-optical networking, nonlinear effects in lasers and photonic waveguides, mid-infrared photonic devices, neuromorphic computing and cryptography at the physical layer. He is a Reviewer for the journals of the IEEE/OSA.

Periklis Petropoulos received the Ph.D. degree in optical telecommunications from the Optoelectronics Research Centre (ORC), University of Southampton. He currently works as a Professor at The University of Southampton. His research interests include in the fields of optical communications, all-optical signal processing and novel fibre, and waveguide technologies. He leads national research projects in these areas. His research has been published extensively in technical journals and conference proceedings, including several invited and post-deadline papers at major international conferences. He has served both as a member and the Sub-Committee Chair of the Technical Programme Committees for several international conferences, including the European Conference on Optical Communication (ECOC) and the Optical Fiber Communication (OFC) Conference. He is the Editor-in-Chief of the *IET Optoelectronics*. Prof Petropoulos is a Fellow of the Optica (formerly the Optical Society of America).